

Study of Dielectric Properties and Ion Transport Parameters in Chitosan-Barium Nitrate Based Solid Polymer Electrolytes

Shujahadeen B. Aziz^{1,2,*}, Shakhawan Al-Zangana³, M. A. Brza^{4,1}, Salah Raza Saeed⁵, Rebar T. Abdulwahid⁶, M. F. Z. Kadir⁷

¹ Prof. Hameeds Advanced Polymeric Materials Research Lab., Department of Physics, College of Science, University of Sulaimani, Qlyasan Street, Sulaimani, Kurdistan Regional Government-Iraq

² Komar Research Center (KRC), Komar University of Science and Technology, Sulaimani, 46001, Kurdistan Regional Government, Iraq

³ Department of Physics, College of Education, University of Garmian, Kalar, 46021, Iraq

⁴ Department of Manufacturing and Materials Engineering, Faculty of Engineering, International Islamic University of Malaysia, Kuala Lumpur, Gombak, Malaysia

⁵ Charmo Research Center, Charmo University, Peshawa Street, Chamchamal, Sulaimani, Kurdistan Region, Iraq

⁶ Department of Physics, College of Education, University of Sulaimani, Kurdistan Regional Government, Old Campus, Sulaimani, Iraq

⁷ Centre for Foundation Studies in Science, University of Malaya, Kuala Lumpur, Malaysia

*E-mail: shujahadeenaziz@gmail.com

Received: 10 July 2019/ Accepted: 8 September 2019 / Published: 29 October 2019

In this report, dielectric properties and ion transport parameters in chitosan (CS) based solid polymer electrolyte (SPE) were examined. In this study, various amount of barium nitrate $\text{Ba}(\text{NO}_3)_2$ was dissolved in CS host polymer to synthesize solid polymer electrolytes (SPEs). The dielectric constant and dielectric loss increased with increasing $\text{Ba}(\text{NO}_3)_2$. On the basis of Trukhan model, the ion transport parameters, such as mobility (μ), diffusion coefficient (D), and charge carrier number density (n) were calculated successfully. Due to higher concentration of salt, enlargement of dielectric loss along with a rise in dielectric constant was perceived. Electrode polarization allowed an extensive dispersion of dielectric constant spectra that transpired at low frequency region. The interesting observation is the loss tangent peaks shifted to higher frequency region and the intensity decreased with an increase in temperature. The increase of μ and D are related to shifting of $\tan\delta$ to high frequency sides with increasing temperature. The decrease of n is correlated with decrease of $\tan\delta$ peak with temperature. The mechanism of ion transport was investigated in the polymer via the $\tan\delta$ spectra. The ion transport parameters are found to be $9 \times 10^{-8} \text{ cm}^2/\text{s}$, $0.8 \times 10^{17}/\text{cm}^3$, and $3 \times 10^{-6} \text{ cm}^2/\text{Vs}$ for D , n , and μ , respectively at ambient temperature. All these parameters have shown increasing as temperature increased. The electric modulus parameters were studied in an attempt to understand the relaxation dynamics and to clarify the relaxation process and ion dynamics relationship.

Keywords: Natural polymer; impedance study; dielectric properties; electric modulus study; ion transport parameters; Trukhan model

1. INTRODUCTION

The extracted ion conducting polymers from inorganic compounds such as dissolved salts in polymers that enrich in functional groups has drawn attention of a number of research groups owing to their applications in solid-state polymer batteries and fuel cells [1-4]. Owing to comparatively greater performance, portability, durability, cost-efficiency, and mechanical flexibility, research and development (R & D) has been carried out on a large scale on solid electrolytes with respect to their utilization in various electrochemical device applications [5-12]. So far, weak conductivity, thermal instability and mechanical deficiency are identified as main attributes of ion conducting polymers [13-15]. To know about ionic conductivity in polymer electrolytes, it is necessary to determine ion mobility, concentration, and diffusion coefficient parameters [16]. In order to study PEO and PVA based polymer electrolytes, these parameters have to be the subject of focus [17-19]. From environmental point of view, chitosan (CS) is well known as an environmentally friendly chemical since it is nontoxic and natural biodegradable polymer membrane [20]. It is apparent, if natural polymers are compared to synthetic ones, the former ones have normal inclination to decay [21]. The deacetylation of chitin produces CS and obtained from the outer skin of the crustaceans, such as shrimps, lobsters, and crabs [22]. To maintain the flexibility and mechanical stability constant across vast temperature range, and reduce the crystalline phases, integration of nano-sized fillers into polymer electrolytes was involved in the methodology of rising electrical conductivity [23-28]. Initially, the most essential element of electrochemical devices is thought to be ion conducting electrolytes. According to documentations, researchers are encouraged to design efficient ion conducting polymer electrolytes because of the ambiguity regarding the method of ion conductivity [29-34]. Moreover, it is also observed that ion transport process proves to be a complex subject in polymer physics.

Nevertheless, it is confirmed that electric property characterizations of priority task before using the electrolytes in electrochemical applications, such as battery and supercapacitor. Based on the DC conductivity of relatively high ion conducting polymer electrolytes, they have been the electrolyte of choice in desired applications [35]. For example, the dielectric behavior of polymer electrolytes is crucial property to collect information about molecular structure of the system [36]. In order to cope up with the relaxation dynamics, degradation, and structure of polymeric systems, it is believed that electrical impedance spectroscopy is probably a great and sensitive technique. Through the research of loss tangent ($\tan\delta$) relaxation peaks and impedance plots, crystalline and amorphous phases of PEO were analyzed in chitosan based blend electrolytes in the previous study [37]. In the best of our knowledge, lost tangent ($\tan\delta$) relaxation peaks have not been applied by any of the research works for determining ion transport parameters in chitosan based electrolytes.

2. EXPERIMENTAL DETAIL

2.1 Materials and sample preparation

Samples are obtained from pure chitosan namely CSBN0 and some others loaded with different concentrations 10% and 20% of barium nitrate $\text{Ba}(\text{NO}_3)_2$. The procedure was started with dissolution of 1 g of CS in 80 mL of 1% acetic acid. Then, the solution was stirred with a magnetic stirrer continuously for several hours till the CS powder has completely dispersed and clear viscose solutions resulted. Afterward, 10 up to 20 wt. % of $\text{Ba}(\text{NO}_3)_2$ were added separately to the CS solution to prepare CS:BaNt polymer electrolyte. This mixture of CS:BaNt was stirred again to gain homogeneous solution. Finally, casting in Petri dish was performed, then each casted sample was left to dry at room temperature to form films and subsequently, the films were then put into desiccators for extra drying and moisture elimination. The samples were coded as CSBN0, CSBN1 and CSBN2 for CS incorporated with 0, 10% and 20% $\text{Ba}(\text{NO}_3)_2$, respectively.

2.2 Electrical impedance spectroscopy (EIS)

Complex impedance spectroscopy (CIS) is a usual method in investigating electrochemical properties of materials which were used in solid-state batteries and this method helps in the identification of the electrical properties of materials at the bulk and their interfacial areas with electronically conducting electrodes. During the sample preparation process, small disk (2.1 cm in width) were produced using the SPE. Meanwhile during sample preparation, the samples were inserted between a couple of stainless steel electrodes subjected to spring pressure for the purpose of measuring impedance through HIOKI 3531 Z Hi-checker. The data obtained was taken via computerized system operating at 50 Hz to 1000 kHz frequency and at temperatures between 303 K and 355 K. In the Nyquist plot, the two parts of the spectra; the real Z' and the imaginary Z'' parts of the complex impedance Z^* were analyzed and shown. Below mentioned equations can be utilized to compute the real and the imaginary parts of permittivity (ϵ^*) and modulus (M^*) [30-35],

$$\epsilon' = \frac{Z''}{\omega C_o (Z'^2 + Z''^2)} \quad (1)$$

$$\epsilon'' = \frac{Z'}{\omega C_o (Z'^2 + Z''^2)} \quad (2)$$

$$\text{Tan}\delta = \frac{\epsilon''}{\epsilon'} \quad (3)$$

$$M' = \frac{\epsilon'}{(\epsilon'^2 + \epsilon''^2)} = \omega C_o Z'' \quad (4)$$

$$M'' = \frac{\epsilon''}{(\epsilon'^2 + \epsilon''^2)} = \omega C_o Z' \quad (5)$$

where vacuum capacitance, that can be acquired by $C_o = \epsilon_o A/t$, is represented by C_o , where the free space permittivity is presented by ϵ_o , the area of the electrode is denoted by A and the sample thickness is represented by t . The angular frequency $\omega = 2\pi f$, where the applied field frequency is denoted

by f . Real part and imaginary part of the complex electric modulus are particularly represented by M' and M'' . Moreover, dielectric constant and dielectric loss are particularly represented by ϵ' and ϵ'' .

3. RESULTS AND DISCUSSION

3.1 Frequency dependence of ϵ' and ϵ''

Figures 1 and 2 exhibits the frequency dependence of dielectric constant and dielectric loss of all the samples, respectively. The high dielectric constants (ϵ') and dielectric loss (ϵ'') over lower frequency regions are normally associated to the buildup of ions at the electrode/electrolyte interfaces of the samples doped with various concentrations of the barium nitrate salt. On this basis, the reduced dielectric constants, at higher frequencies, are correlated to the reduction in polarization as a result of the ions accumulation [6,38-40]. In a comparison, the doped chitosan samples showed higher dielectric constant than the pure sample.

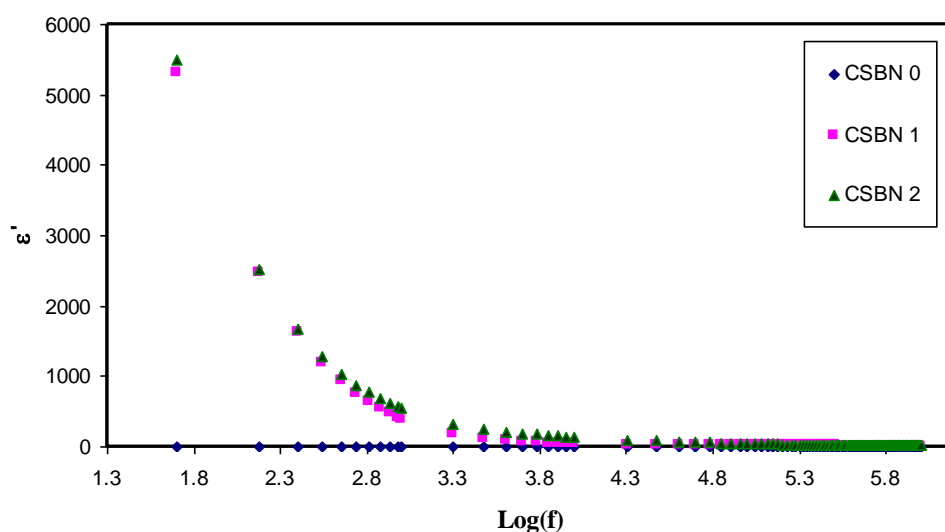


Figure 1. Frequency dependence of dielectric constant (ϵ') for CSBN0, CSBN1, and CSBN2 samples at ambient temperature.

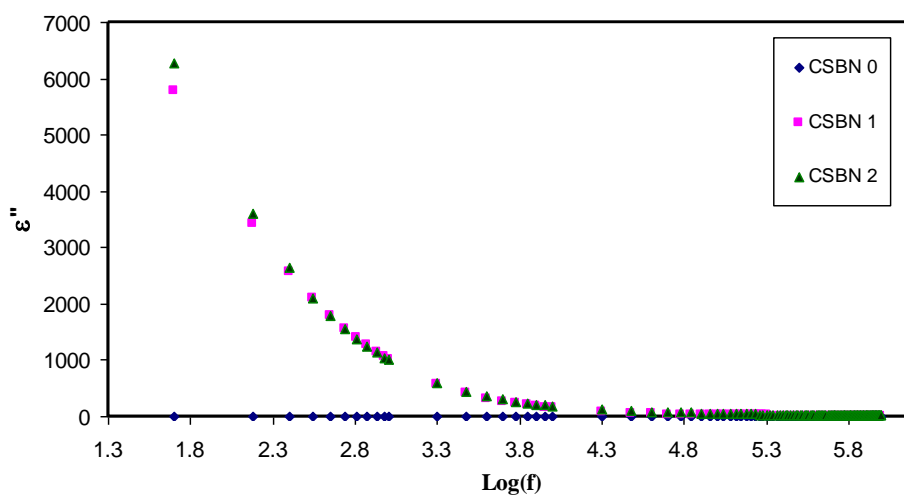


Figure 2. Frequency dependence of dielectric loss (ϵ'') for CSBN0, CSBN1, and CSBN2 samples at ambient temperature.

The fact that the dielectric constant and dielectric loss value attain highest for 20 wt. % Ba/Nt salt can be illustrated by Figures 1 and 2. It is well reported that three factors, like degree of salt dissociation (concentration of ion), ion mobility, and dielectric constant control the range of ion transfer in polymer electrolytes and nanocomposites [41]. Formerly, it was illustrated that dielectric constant (ϵ') and charge carriers number density (n_i) are vigorously interconnected via this relation: $n_i = n_o \exp(-U/\epsilon KBT)$, representing U as the dissociation energy [7,24,26,31]. Thus, a fall in dielectric constant is followed by a fall in DC conductivity. The linkage can be lengthened to that the DC ionic conductivity of polymer ion-conductivity electrolytes relies on the number density of ions (n_i) and mobility of ions (μ_i) ($\sigma = \sum qn_i\mu_i$), representing q as the charge carrier of ions [7,24,26,31,42]. Thus, in order to comprehend the electrical properties of polymer electrolytes, researching about the dielectric constant might be reviewed as an informative and useful parameter. Conductivity behavior of the samples might also be guessed from this.

Ultimately, whatever discussed convinced us that ion transport properties such as DC conductivity, mobility, charge carrier density, and dielectric parameters strongly interrelated. Accordingly, it is shown that in the next sections these transport parameters can be obtained from the dielectric properties. Figure 3 shows a clear shift of the loss tangent ($\tan\delta$) peaks to higher frequency side with increasing salt concentration. As a consequence, 20 wt. % of salt concentration dissolution in the sample exhibits the highest conductivity.

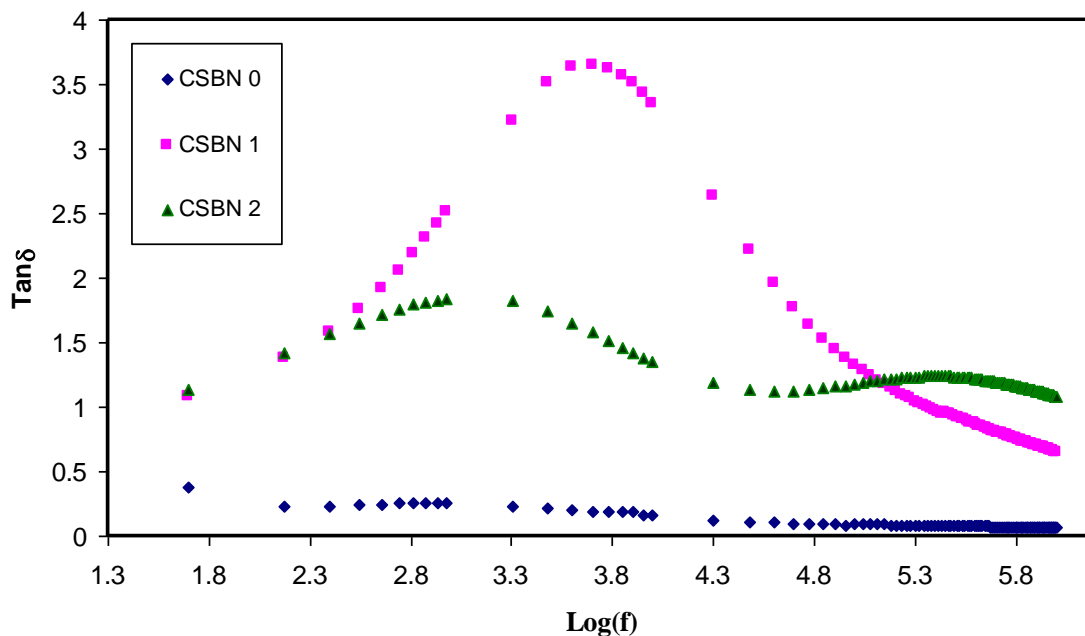


Figure 3. Frequency dependence of loss tangent for CSBN0, CSBN1, and CSBN2 samples at room temperature.

3.2 Dielectric properties as a function of temperature

The dielectric constant and dielectric loss as a function of frequency for CSBN2 film at various temperatures as presented in Figures 4 and 5. At the low frequency region, the highest values of ϵ' obtained whereas the values declined as the frequency increasing. The former case can be explained on basis of Maxwell-Wagner model [43]. It was also studied that the dielectric constant has shown higher values as temperature increased for CSBN2 sample. The increase of ϵ' with increasing temperature is ascribed to this quick orientation of the dipoles in CS which resulted in enhancing the mobility of charge carriers [6,11,39].

Both figures show a general trend that as the temperature increases, the permittivity increases as well. In fact, temperature increasing facilitates dipole orientation process. Also, it causes charge carrier density increasing as a result of increasing salt dissociation and dissolution. These behaviors occur in several polymer electrolytes as shown in the literature [44-46]. It is vital mentioning that primary, also known as intra-chain and secondary, also known as inter-chain are two presence forces in polymer materials which lead to the stability of polymer structure [47]. Dipole-dipole bonding (0.43-0.87 eV), hydrogen bonding (0.13-0.30 eV), induced interaction (0.07-0.13 eV), and dispersion interaction (0.002-0.09 eV) are the four varying secondary forces. Moreover, the primary force is reflected in the creation of covalent bond (2.2-8.6 eV) which contributes in binding the backbone chains together. It must be noted that the secondary forces have comparatively little dissociation energies than the primary ones while discussing the susceptibility to temperature change.

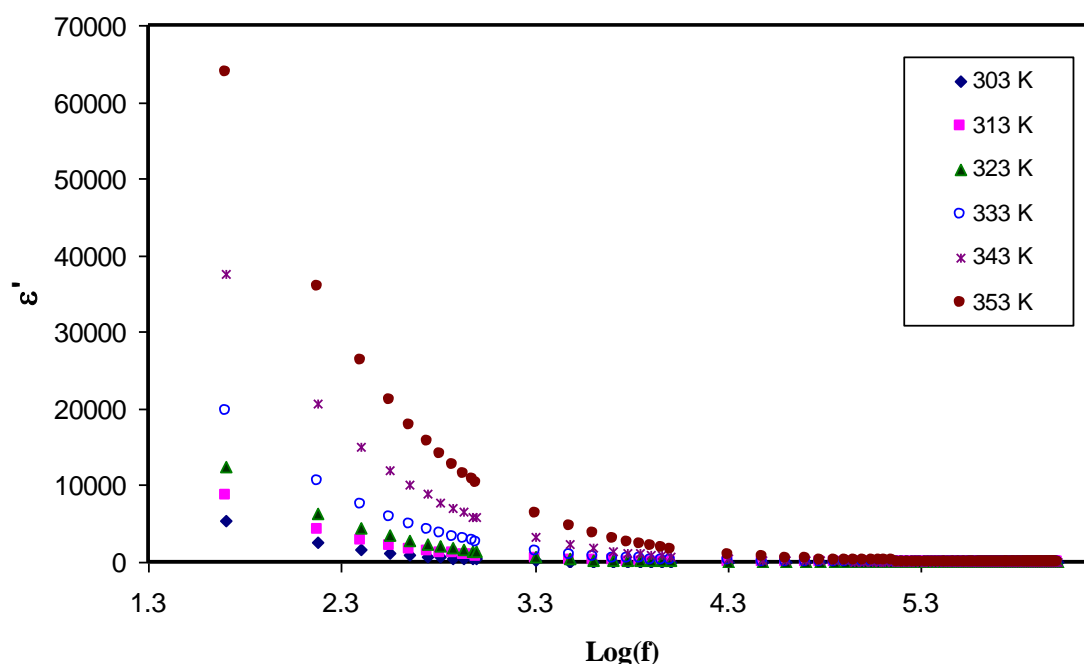


Figure 4. Frequency dependence of dielectric constant ϵ' for CSBN2 sample at various temperature.

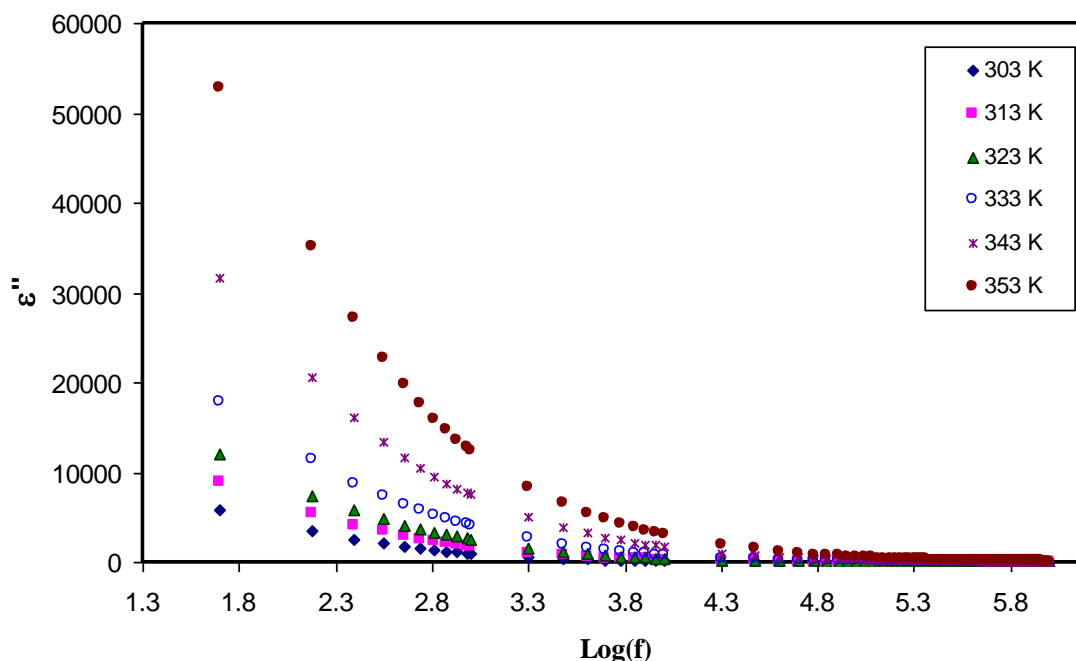


Figure 5. Frequency dependence of dielectric loss (ϵ'') for CSBN2 sample at various temperature.

3.3 Electric Modulus Study

Figure 6 shows spectra of real part of the electric modulus M' for all the samples at ambient temperature. From the curves there is an increase of M' with frequency increasing and kept continuing as the frequency increases. It is worth-noticing the maximum peak moves to the higher frequency in the spectra and out of the range of the present experiment. Variation of M'' values with frequency for all the samples at ambient temperature is shown in Figure 7. It is interesting that a distinct peak is observed for the pure CSBN0 sample at the middle frequency region. Accordingly, it is clear that this peak has almost symmetric appearance on both sides of the maxima and predictable from ideal Debye manner. More interesting thing is the disappearance of the peak in the frequency range of our experiment, which is probably moved towards higher frequency region.

In order to comprehend the bulk relaxation properties in regions characterized with low frequencies, seemingly, researchers receive a great assistance by utilizing electric modulus. Activity like unclear relaxation in dielectric permittivity demonstration that is generated by three general problems i.e. Electrode polarization, phenomena of space charge injection, and conduction effects, is likely to be settled in electric modulus formalism [32,34,35,37]. Figure 8 shows the real part M' of electrical modulus as a function of frequency for the CSBN2 sample at various temperature. It is obvious from Figure 8 that an M' spectrum reveals a long tail at low frequency region, meaning a great reliance of capacitance on the SPE [48].

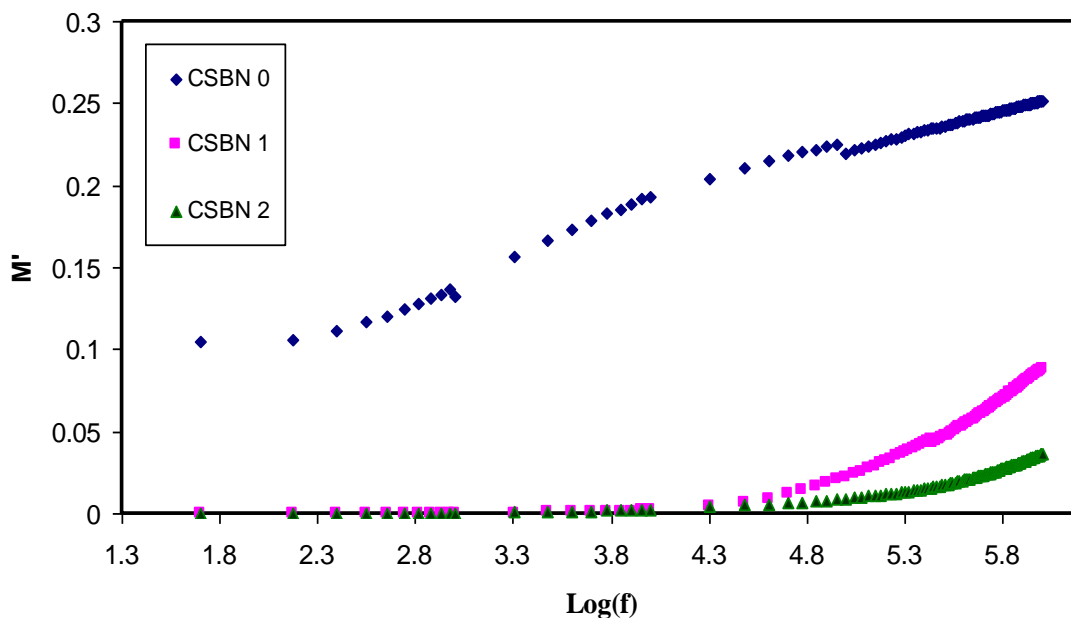


Figure 6. Frequency dependence of real part of electric modulus M' for CSBN0, CSBN1, and CSBN2 samples.

Figure 9 illustrates the imaginary part M'' of electric modulus as a function of frequency for the CSBN2 sample at various temperature. Relaxation peak at reduced temperatures, that can be seen evidently from the M'' spectra, verifies the combination of ionic movements and polymer segmental motions in the polymer electrolyte which indicates peak in the M'' spectra [49] without any corresponding feature in the spectra of ϵ'' . These peaks specify transition regions from long range ionic mobility (translation) to short range of dipolar mobility, i.e., the charge carriers are restricted to potential wells and are forced to move within a small distance at extensive frequency region [50]. The impact of temperature and reduction of conductivity relaxation time at high temperatures is specified when a rise in temperature shows the forward movement of maximum peak with this frequency region of the M'' spectra.

In a contrasting situation, permittivity rises and M' falls with rise in temperature. M' values decline (ϵ' rises) as a result of the enlarged mobility of the polymer segment and charge carriers along with a rise in temperature. Equations 4 and 5 can strongly verify that due to conductivity modification, Z' and Z'' fall. Disparity in M'' values over frequency range at different temperatures for CSBN2 sample is illustrated by Figure 9.

The graphical demonstrations of the spectra of M'' enables us to analysis of conductivity via its peak on frequency axis. At lower frequency regions, the value of M'' is low relative to the higher frequency ones, which might be owing accumulation of ions and thus the enhanced capacitance formation at the interfacial region [51].

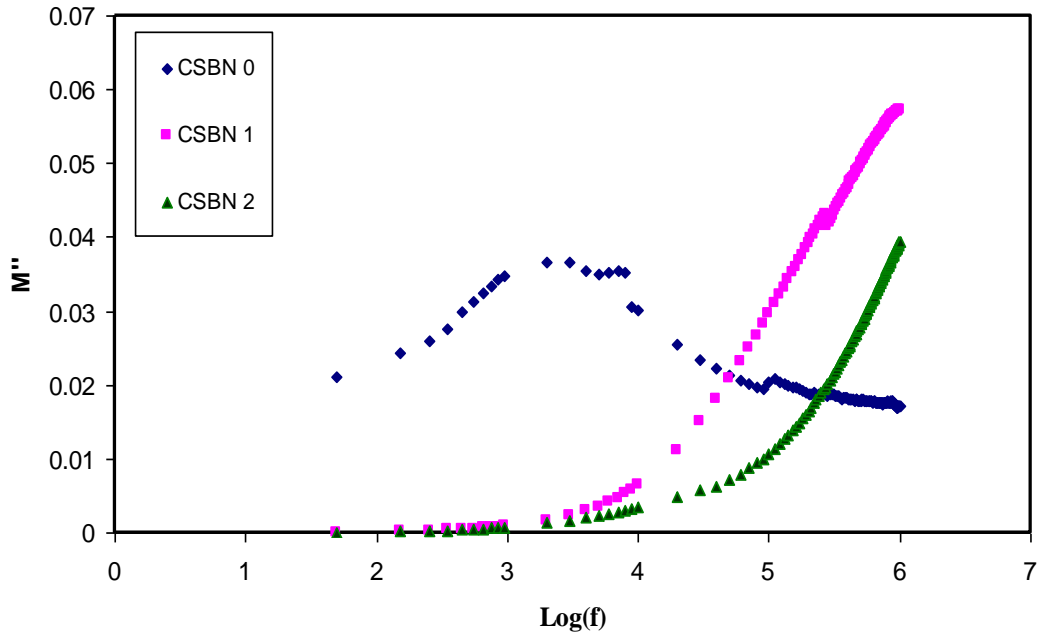


Figure 7. Frequency dependence of imaginary part of electric modulus M'' for CSBN0, CSBN1, and CSBN2 samples

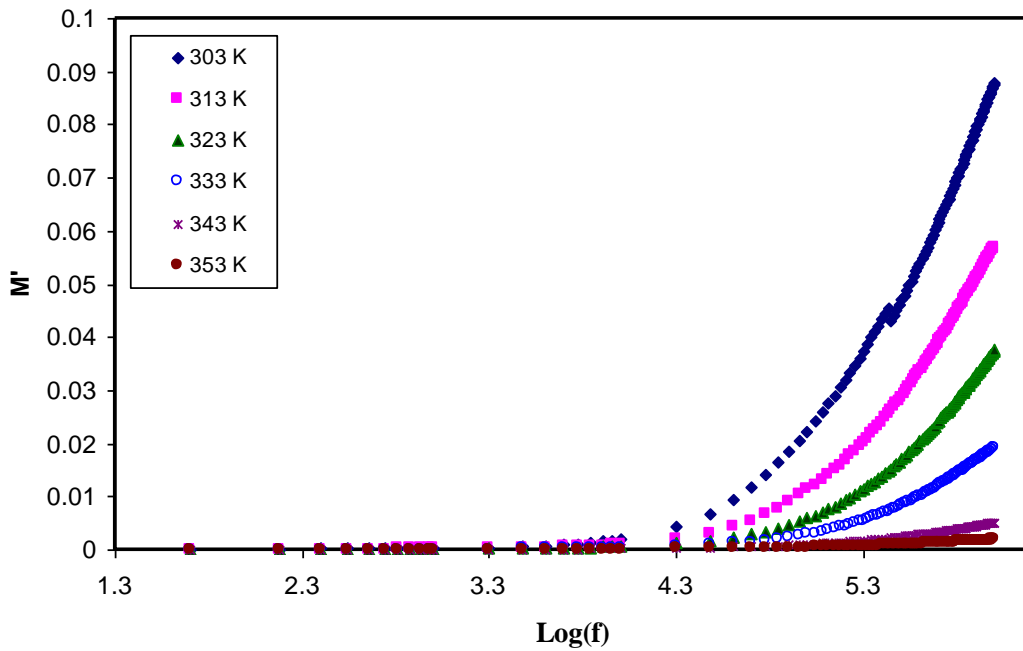


Figure 8. Frequency dependence of real part of electric modulus M' for CSBN2 sample at various temperature.

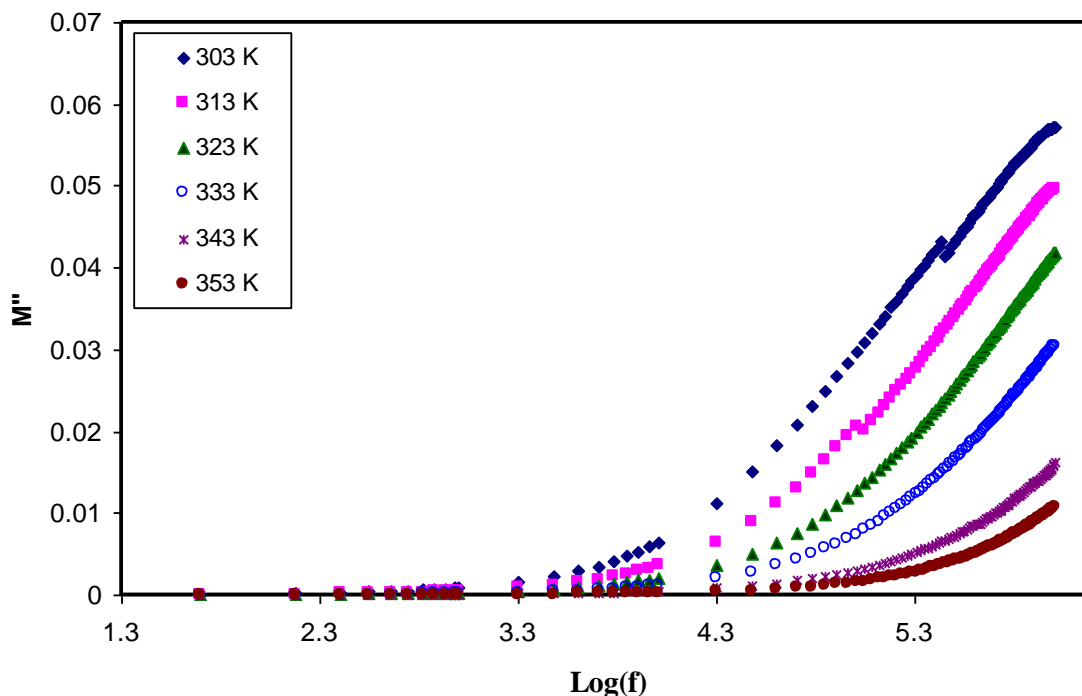


Figure 9. Frequency dependence of imaginary part of electric modulus M'' for CSBN2 sample at various temperature.

3.4 Loss tangent and Ion Transport Study

The process of the ion conduction remains incomprehensible in the SPEs as there is a concurrent presence of crystalline and amorphous phases. Thus, along with the processes of polymer segmental relaxation in polymer electrolytes [35,37,52,53], it is impressive to comprehend this process of ion transfer. The process of ion transfer remains an arguable subject till date, among the researchers. Dielectric loss tangent is the ratio ϵ'' to ϵ' ($\tan(\delta) = \frac{\epsilon''}{\epsilon'}$).

The loss tangent as a function of the logarithm of frequency at various temperatures for CS:Ba(NO₃)₂ (CSBN2) is presented in Figure 10. From this figure, one can notice the loss tangent increasing with frequency increasing till a peak appearance; subsequently it decreases with increasing frequency. Another notice is that both the position as well as the height of the peak increase with increase in temperature. It is self-evident that as the temperature increases, the charge carrier movement facilitates and thereby capable of relaxation at higher frequencies [54]. Koops phenomenological model explains the $\tan \delta$ shape of Figure 10 [55]. Since the ohmic component of current increases at a faster rate than the capacitive component, loss tangent raises with rise in frequency, and reaches maximum at a particular frequency at different temperatures. However, on contrary, this is associated to the capacitive component ($Z_i = 1/2\pi fC$) and insignificant at low frequency. Moreover, the loss tangent sees a decline as the frequency goes higher since the ohmic component of current does not depend on frequency. This is because of the high value of frequency and therefore enhancement in capacitive component with rise in frequency [56,57]. The whole discussion makes us to realize that the shape and intensity of $\tan(\delta)$ peaks at various temperatures are definitely correlated to the ion transport parameters, such as mobility and

diffusion. The values of $\tan(\delta)_{max}$ and frequency can be used to draw plots of mobility (μ), carrier density (n), and diffusivity (D) as a function of temperature, which will be discussed in the next sections.

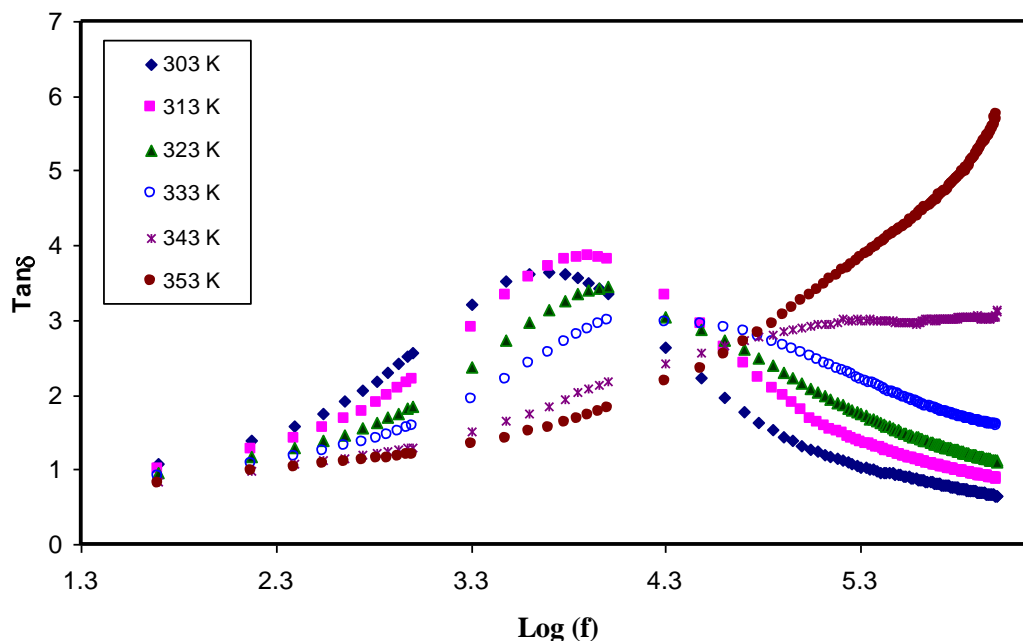


Figure 10. Frequency dependence of loss tangent for CSBN2 sample at various temperature.

The correlation of the shape of $\tan\delta$ plots to the capacitive and resistive components of the solid electrolysis shown in loss tangent study. Furthermore, the shifting of $\tan\delta$ peaks towards the high frequency side is explained on the basis of the fact that the ions are thermally activated. Implementation of the Trukhan model to the loss tangent data was carried out in the calculation of the number density, mobility, and diffusion coefficient of the charge carriers. From this model, diffusion coefficient of cations and anions are supposed to be the same so that a simple expression can be used in calculation of the diffusion coefficient from the peaks appeared in the plots of loss tangent versus frequency. The expression is shown below:

$$D = \frac{2\pi f_{max} L^2}{32 \tan^3(\delta)_{max}} \quad (6)$$

Where: L is the sample thickness [58].

Diffusion coefficient as a function of temperature is presented in Figure 11. It is noticed that the diffusion coefficient increases with the temperature non-linearly. This belonged to taken into consideration of segmental motion in the diffusion process [59], and also temperature increasing favors diffusion of segmental motion.

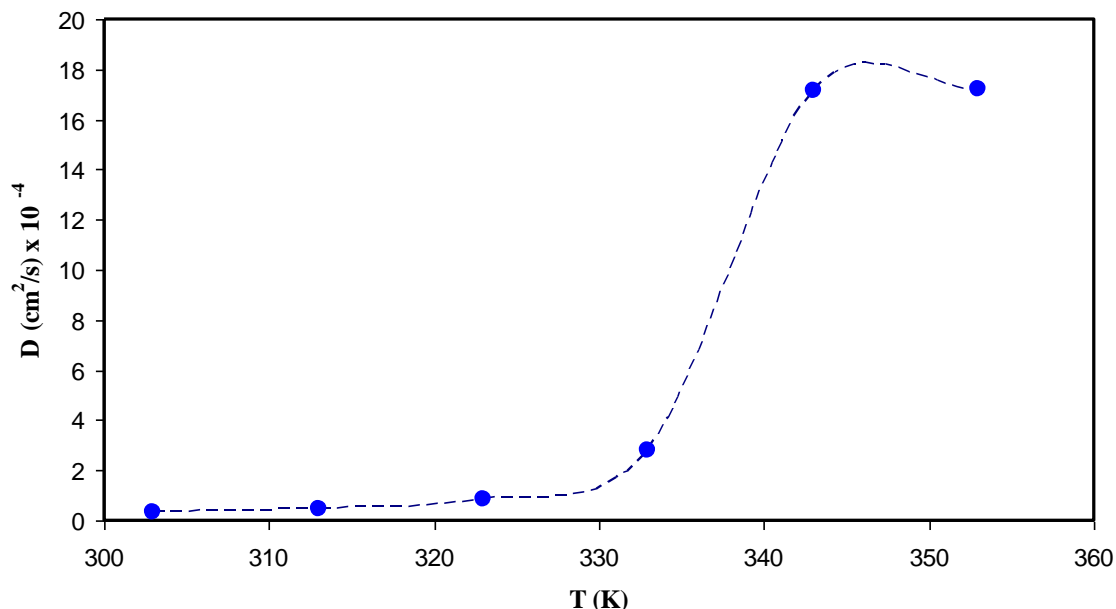


Figure 11. Temperature dependence diffusion coefficient for CSBN2 sample.

The number of density of mobile ions is another important parameter that in relation to conductivity. Estimation of the number density of mobile ions (n) from the well known Einstein equation is performed [58]:

$$n = \frac{\sigma_{DC} K_B T}{D e^2} = \left(\frac{\sigma_{DC} K_B T}{e^2} \right) \left[\frac{32 \tan^3 \delta_{max}}{2\pi f_{max} L^2} \right] \quad (7)$$

where: σ is obtained from impedance plots, K_B , T , D , and e have usual meaning. It is obviously seen that charge carrier density is directly and inversely proportional to cubic of $\tan \delta_{max}$ value and to the shifting of peak frequencies, respectively. It is also verified that $\tan \delta_{max}$ values do not change largely if their intensity do not change significantly and thus the carrier density becomes almost constant.

Figure 12 exhibits the plot of n as a function of temperature. Accordingly, there is an increase in n as temperature increases; however, it remains less than an order of magnitude. The influence of temperature is explained by considering the ions held in the crystalline parts of the polymer matrix can be released by making the polymer more amorphous the temperature increased.

Agrawal et al. [60] have demonstrated the ion concentration in the range of 10^{15} to $10^{16}/\text{cm}^3$ for PEO:AgNO₃:SiO₂ system. It is also reported that the conductivity is reliant on the mobile ions number and mobility [60]. In the current work, the values of the charge carrier density of $(0.7-3.7) \times 10^{14}/\text{cm}^3$ were achieved and are in comparable to those reported for SPEs in the literature [60,61].

Ion mobility is also another parameter that can be computed from the following equation:

$$\mu = \frac{\sigma_{DC}}{en} = \frac{De}{K_B T} = \left(\frac{e}{K_B T} \right) \left[\frac{2\pi f_{max} L^2}{32 \tan^3 \delta_{max}} \right] \quad (8)$$

Where: μ is the ionic mobility.

Figure 13 shows the relationship between temperature and ion mobility. Similarly, both μ and diffusivity are strongly dependent on temperature. It is interesting to note that as the temperature increased, there an increase in the ion mobility but this increase is not linear. Free volume model can explain the increase in the ion mobility on the basis of the existence of free volume that enlarged in the amorphous region as the temperature increased. [56].

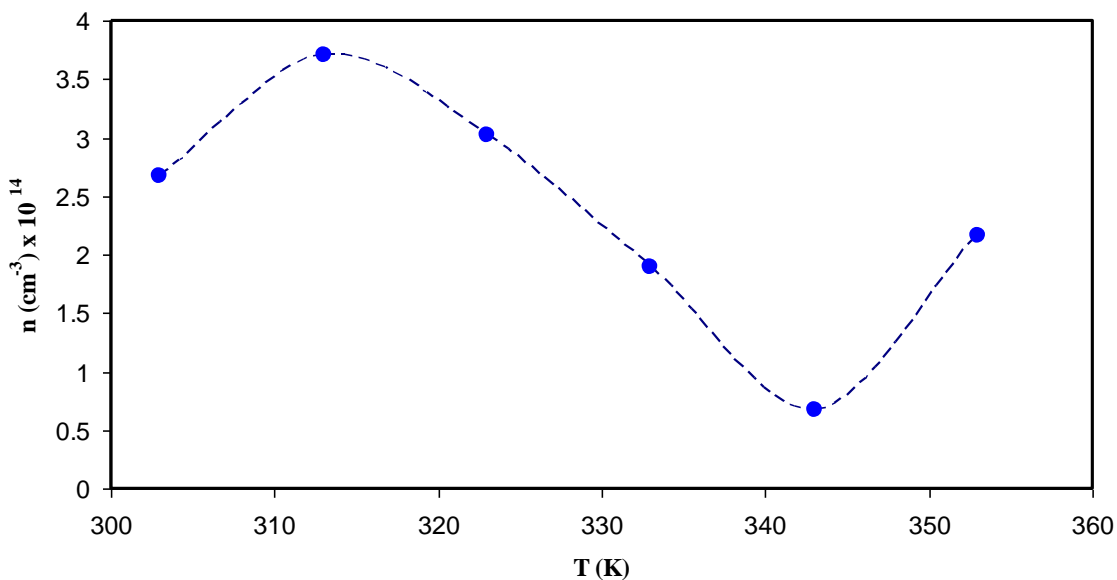


Figure 12. Temperature dependence carrier density for CSBN2 sample.

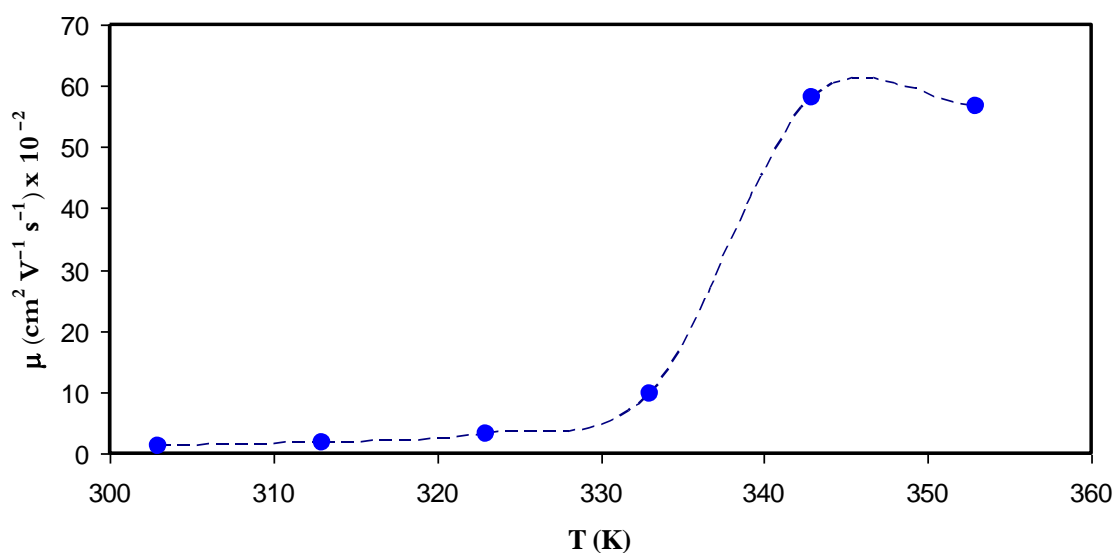


Figure 13. Temperature dependence carrier mobility for CSBN2 sample.

In the current work, the values of the ion mobility of $(1-60) \times 10^{-2} \text{ cm}^2/\text{Vs}$ were achieved and quite large compared to those obtained for SPEs in the literature. For example, the values of ion mobility have been determined to be $1.5 \times 10^{-3} \text{ cm}^2/\text{Vs}$ at ambient temperature, whereas it is about $2.8 \times 10^{-2} \text{ cm}^2/\text{Vs}$ at

353 K. Agrawal et al. [60] documented various value of $10^{-3} \text{cm}^2/\text{Vs}$ for ionic mobility. Winie et al. [62] have also settled such direct proportionality connection between mobility of ions and temperature. Numerous researchers have reported results on the mobility of ion. For example, Majid and Arof [63] demonstrated that the mobility values were in the range of 10^{-8} to $10^{-6} \text{cm}^2/\text{Vs}$. Moreover, Arya and Sharma [64] demonstrated that the mobility of ions were in the range of 10^{-10} to $10^{-12} \text{cm}^2/\text{Vs}$.

4. CONCLUSIONS

In conclusion, the dielectric properties and ion transport parameters in chitosan (CS) based SPE were explored. Application of Trukhan model was carried out in calculation of ion transport parameters successfully. Addition of various amount of barium nitrate $\text{Ba}(\text{NO}_3)_2$ into CS host polymer was performed to fabricate SPEs. The dielectric constant and dielectric loss increased with addition of $\text{Ba}(\text{NO}_3)_2$. The increase of dielectric constant and dielectric loss were observed with increasing salt concentration. Electrode polarization caused an extensive dispersion of the spectra of dielectric constant at low frequency region. On the basis of Trukhan model, the ion transport parameters, such as mobility (μ), diffusion coefficient (D), and charge carrier number density (n) were calculated successfully. The interesting observation is the loss tangent peaks shifted to higher frequency region and the intensity decreased with an increase in temperature. The increase of μ and D are related to shifting of $\tan\delta$ to high frequency sides with increasing temperature. The decrease of n is correlated with decrease of $\tan\delta$ peak with temperature. The mechanism of ion transport was investigated in the polymer via the $\tan\delta$ spectra. The ion transport parameters are found to be $9 \times 10^{-8} \text{cm}^2/\text{s}$, $0.8 \times 10^{17}/\text{cm}^3$, and $3 \times 10^{-6} \text{cm}^2/\text{Vs}$ for D , n , and μ , respectively at ambient temperature. All these parameters have shown increasing as temperature increased. The electric modulus parameters were studied in an attempt to understand the relaxation dynamics and to clarify the relaxation process and ion dynamics relationship.

ACKNOWLEDGEMENT

The authors gratefully acknowledge the financial support from the Kurdistan National Research Council (KNRC)- Ministry of Higher Education and Scientific Research-KRG. The authors also acknowledge the University of Sulaimani, and the Komar University of Science and Technology for providing the facility and financial support to carry out this work.

References

1. M. Malathi, K. Tamilarasan and V. Ganesan, *Polym. Compos.*, 36 (2015) 42.
2. T. Osaka, *J. Electrochem. Soc.*, 141 (1994) 1994.
3. Y. Jiang, X. Yan, Z. Ma, P. Mei, W. Xiao, Q. You and Y. Zhang, *Polymers*, 10 (2018) 1.
4. R.C. Agrawal and G. P. Pandey, *J. Phys. D. Appl. Phys.*, 41 (223001) 2008.
5. A. Eftekhari, Ed., Cambridge: Royal Society of Chemistry, 2019. ISBN: 978-1-78801-418-2
<https://doi.org/10.1039/9781788016124>
6. S. B. Aziz, M. H. Hamsan, M. F.Z. Kadir, W. O. Karim, R. M. Abdullah, *Int. J. Mol. Sci.*, 20 (2019) 3369.
7. S.B. Aziz, M.A. Rasheed and Z. H. Z. Abidin, *J. Electron. Mater.*, 46 (2017) 6119.
8. M.H. Hamsan, S. B. Aziz, M.F. Shukur, M.F.Z. Kadir, *Ionics*, 25 (2019) 559.

9. S. B. Aziz, O.G. Abdullah, S. R. Saeed and H. M. Ahmed, *Int. J. Electrochem. Sci.*, 13 (2018) 3812.
10. S.B. Aziz, S. Al-Zangana, H.J. Woo, M.F.Z. Kadir and O.G. Abdullah, *Results Phys.*, 11 (2018) 826.
11. S. B. Aziz, M.H. Hamsan, R. M. Abdullah, M.F.Z. Kadir, *Molecules*, 24 (2019) 2503.
12. H. Duan, M. Fan, W.-P. Chen, J.-Y. Li, P.-F. Wang, W.-P. Wang, J.-L. Shi, Y.-X. Yin, L.-J. Wan and Y.-G. Guo, *Adv. Mater.*, 31 (2019) 1807789.
13. C.R. Pila, E.P. Cappe, N.D.S. Mohallem, O.L. Alves, M.A.A. Frutis, N. Sánchez-Ramírez, R.M. Torresi, H.L. Ramírez and Y.M. Laffita, *Solid State Sci.*, 88 (2019) 41.
14. P.M. Ketkar, K.-H. Shen, L.M. Hall and T.H. Epps, *Mol. Syst. Des. Eng.*, 4 (2019) 223.
15. N.S. Schausser, R. Seshadri and R. A. Segalman, *Mol. Syst. Des. Eng.*, 4 (2019) 263.
16. M. Siekierski, W. Wiczorek and J. Przyłuski, *Electrochim. Acta*, 43 (1998) 1339.
17. L.R.A.K. Bandara, M. A.K. L. Dissanayake and B.-E. Mellander, *Electrochim. Acta*, 43 (1998) 1447.
18. R.J.Klein, S. Zhang, S. Dou, B.H. Jones, R.H. Colby and J. Runt, *J. Chem. Phys.*, 124 (2006) 144903.
19. H.A. Every, F. Zhou, M Forsyth and D.R. MacFarlane, *Electrochim. Acta*, 43(1998) 1465.
20. L. Cao, M. Yang, D. Wu, F. Lyu, Z. Sun, X. Zhong, H. Pan, H. Liu and Z. Lu, *Chem. Commun.*, 53 (2017) 1615.
21. N.S. Salleh, S.B. Aziz, Z. Aspanut and M.F.Z. Kadir, *Ionics (Kiel)*, 22 (2016) 2157.
22. I. Fauzi, I. M. Arcana, *AIP Conf. Proc.*, 1589 (2014) 154.
23. S.B. Aziz, *Appl. Phys. A*, 122 (2016) 706.
24. S.B. Aziz, *Adv. Mater. Sci. Eng.*, 2016(2016)1.
25. S.B. Aziz, M.A.Brza, P.A. Mohamed, M.F.Z. Kadir, M.H.Hamsan, R.T. Abdulwahid and H.J. Woo, *Results in Physics*, 13 (2019) 102326.
26. S.B. Aziz and Z.H.Z. Abidin, *J. Appl. Polym. Sci.*, 132 (2015) 41774.
27. M. Tomczykowa, M. Plonska-Brzezinska, M. Tomczykowa and M. E. Plonska-Brzezinska, *Polym.(Basel)*, 11 (350) 2019.
28. P. B. Sassmann and O. Weichold, *Ionics*, 25 (2019) 3971.
29. S.B. Aziz and Z.H.Z. Abidin, *Mater. Chem. Phys.*, 144 (2014) 280.
30. S.B. Aziz and S. M.Mamand, *Int. J. Electrochem. Sci.*, 13(2018)10274.
31. S.B. Aziz, *Iran Polym J*, 22 (2013) 877.
32. S.B. Aziz, Z.H.Z. Abidin and A. K. Arof, *eXPRESS Polym.*, 4 (2010) 300.
33. S.B. Aziz, T.J. Woo, M.F.Z. Kadir and H.M. Ahmed, *J. Sci.: Adv. Mater. Devices*, 3 (2018) 1.
34. S.B. Aziz, *J Inorg Organomet Polym*, 28 (2018)1942.
35. S.B. Aziz, R.M. Abdullah, M.F.Z. Kadir and H.M Ahmed, *Electrochim. Acta*, 296 (2019) 494.
36. Z. Lu, M. Lanagan, E. Manias and D. Macdonald, *ECS Trans.*, 28(2010) 95.
37. S.B Aziz and R.M Abdullah, *Electrochim. Acta*, 285 (2018) 30.
38. S. Al-Zangana, M. Iliut, G. Boran, M. Turner, A. Vijayaraghavan and I. Dierking, *Sci. Rep.*, 6(2016) 31885.
39. S.B. Aziz, W.O. Karim, K.W. Qadir and Q. Zafar, *Int. J. Electrochem. Sci.*, 13 (2018) 6112.
40. M.H. Hamsan, M.F. Shukur, S.B. Aziz, M.F.Z. Kadir, *Bull. Mater. Sci.*, 42 (2019) 57.
41. D.K. Pradhan, R.N.P. Choudhary and B. K. Samantaray, *Int. J. Electrochem. Sci.*, 3 (2008) 597.
42. S.B. Aziz, M.F.Z. Kadir and Z.H.Z. Abidin, *Int. J. Electrochem. Sci.*, 11 (2016) 9228.
43. T.T.N. Vu, G. Teyssedre, S. Le Roy and C. Laurent, *Technologies*, 5 (2017) 27.
44. H.J. Woo, S.R. Majid and A.K. Arof, *Mater. Chem. Phys.*, 134 (2012) 755.
45. M. Ravi, Y. Pavani, K.K. Kumar, S. Bhavani, A.K. Sharma and V.V.R. N.Rao, *Mater. Chem. Phys.*, 130 (2011) 442.
46. A.R. Polu, R. Kumar, *Bull Mater Sci.*, 34(2011) 1063.
47. D.K. Das-Gupta, *J. Electrostat.*, 51 (2001) 159.

48. S.L. Agrawal, M. Singh, M. Tripathi, M.M. Dwiedi and K. Pandey, *J Mat Sci.*, 44 (2009) 6060.
49. R.J. Sengwa, S. Choudhary and S. Sankhla, *eXPRESS Polym. Lett.*, 2 (2008) 800.
50. J. Castillo, M. Chacon, R. Castillo, R.A. Vargas, P.R. Bueno and J.A. Varela, *Ionics*, 15 (2009) 537.
51. S.B. Aziz, M.A. Rasheed and Z.H.Z. Abidin, *J. Electron. Mater.*, 46 (2017) 6119.
52. U. Hyeok Choi, S. Liang, Q. Chen, J. Runt and R.H. Colby, *ACS Appl. Mater. Interfaces*, 8 (2016) 3215.
53. S.B. Aziz, R.M. Abdullah, M.A. Rasheed and H.M. Ahmed, *Polymers (Basel)*, 9 (2017) 338.
54. A.L. Saroj and R.K. Singh, *J. Phys. Chem. Solids*, 73 (2012) 162.
55. P. Khatri, B. Behera, V. Srinivas and R.N.P. Choudhary, *Curr. Appl. Phys.*, 9 (2009) 515.
56. B. Louati, F. Hlel and K. Guidara, *J. Alloy. Compd.*, 486 (2009) 299.
57. N.H. Idris, H.B. Senin and A.K. Arof, *Ionics*, 13 (2007) 213.
58. A. Munar, A. Andrio, R. Iserte and V. Compañ, *J. Non-Cryst. Solids*, 357, (2011) 3064.
59. T.S. Tiong, M.H. Buraidah, L.P. Teoet and A.K. Arof, *Ionics*, 22 (2016) 2133.
60. R.C. Agrawal, A. Chandra, A. Bhatt and Y.K. Mahipal, *NJP*, 10 (2008) 043023.
61. A. Chandra, R.C. Agrawal and Y.K. Mahipal, *J. Phys. D: Appl. Phys.*, 42 (2009) 135107.
62. T. Winie, S. Ramesh and A.K. Arof, *Physica B*, 404 (2009) 4308.
63. S.R. Majid, A.K. Arof, *Physica B*, 355(2005) 78.
64. A. Arya and A.L. Sharma, *J Solid State Electrochem.*, 22 (2018) 2725.

© 2019 The Authors. Published by ESG (www.electrochemsci.org). This article is an open access article distributed under the terms and conditions of the Creative Commons Attribution license (<http://creativecommons.org/licenses/by/4.0/>).